HHS Public Access

Author manuscript

Nature. Author manuscript; available in PMC 2018 January 23.

Published in final edited form as:

Nature. 2017 July 20; 547(7663): 364–368. doi:10.1038/nature22988.

K_{2P}2.1(TREK-1):activator complexes reveal a cryptic selectivity filter binding site

Marco Lolicato[1], **Cristina Arrigoni**[1], **Takahiro Mori**[2], **Yoko Sekioka**[2], **Clifford Bryant**[3], **Kimberly A. Clark**[1], and **Daniel L. Minor Jr.**[1,4,5,6,7,*]

[1]Cardiovascular Research Institute, University of California, San Francisco, California 93858-2330 USA

[2]Ono Pharmaceutical, Co. Ltd., Mishima-Gun, Osaka, 618-8585 JAPAN

[3]Small Molecule Discovery Center, University of California, San Francisco, California 93858-2330 USA

[4]Departments of Biochemistry and Biophysics, and Cellular and Molecular Pharmacology, University of California, San Francisco, California 93858-2330 USA

[5]California Institute for Quantitative Biomedical Research, University of California, San Francisco, California 93858-2330 USA

[6]Kavli Institute for Fundamental Neuroscience, University of California, San Francisco, California 93858-2330 USA

[7]Molecular Biophysics and Integrated Bio-imaging Division, Lawrence Berkeley National Laboratory, Berkeley, CA 94720 USA

Abstract

Polymodal K_{2P} (*KCNK*) thermo- and mechanosensitive TREK[1] potassium channels, generate 'leak' currents that regulate neuronal excitability, respond to lipids, temperature, and mechanical stretch, and influence pain, temperature perception, and anesthetic responses[1–3]. These dimeric

*Correspondence to: daniel.minor@ucsf.edu.
Correspondence and requests for material should be made to D.L.M.

Competing financial interests statement

M.L. C.A. K.A.C, C.B., and D.L.M. declare no financial interests.
T.M and Y.S. are employees of Ono Pharmaceutical, Co. Ltd.

Extended Data Material

Methods, along with Extended data figures and tables are found in the Extended Data material document.

Data deposition statement

K_{2P}2.1(TREK-1), 5VK5; K_{2P}2.1(TREK-1):ML335, 5VKN; and K_{2P}2.1(TREK-1):ML402, 5VKP coordinates and structure factors are available at the RCSB.

Author contributions

M.L., C.A. C.B. and D.L.M. conceived the study and designed the experiments. T.M. and Y.S. conceived and ran thallium flux assays. M.L. and C.A. performed experiments. M.L. and K.A.C. expressed and purified proteins. M.L. performed crystallization and structure determination. M.L. and C.A. performed electrophysiological experiments and analyzed the data. C.B. designed synthetic routes, synthesized, and purified the compounds. D.L.M analyzed data and provided guidance and support. M.L., C.A., and D.L.M. wrote the paper.

voltage-gated ion channel (VGIC) superfamily members have a unique topology comprising two pore forming regions per subunit[4–6]. Contrasting other potassium channels, K_{2P}s use a selectivity filter 'C-type' gate[7–10] as the principal gating site. Despite recent advances[3,11,12], K_{2P}s suffer from a poor pharmacologic profile limiting mechanistic and biological studies. Here, we describe a new small molecule TREK activator class that directly stimulates the C-type gate by acting as molecular wedges that restrict interdomain interface movement behind the selectivity filter. Structures of K_{2P}2.1(TREK-1) alone with two selective K_{2P}2.1(TREK-1) and K_{2P}10.1(TREK-2) activators, an *N*-aryl-sulfonamide, ML335, and a thiophene-carboxamide, ML402, define a cryptic binding pocket unlike other ion channel small molecule binding sites and, together with functional studies, identify a cation-π interaction that controls selectivity. Together, our data unveil a previously unknown, druggable K_{2P} site that stabilizes the C-type gate 'leak mode' and provide direct evidence for K_{2P} selectivity filter gating.

K_{2P}2.1(TREK-1)$_{cryst}$ (Extended Data Fig. 1a,b) crystallized alone and with activators, ML335 (N- [(2,4-dichlorophenyl)methyl]-4-(methanesulfonamido) benzamide) and ML402 (N- [2- (4-chloro-2-methylphenoxy)ethyl]thiophene-2-carboxamide), and diffracted X-rays to 3.1 Å, 3.0 Å and 2.8 Å, respectively (Extended Data Table 1) enabling structure determination (Extended Data Fig. 1c). K_{2P}2.1(TREK-1)$_{cryst}$ has a domain-swapped M1 helix, extracellular CAP domain, and an unimpeded aqueous path between the intracellular side and selectivity filter, similar to prior TREK subfamily structures[6,13–15] (Fig. 1a). Features absent in prior K_{2P} structures include a C-terminal tail (C-tail) five helical turns longer than in K_{2P}10.1(TREK-2)[6], Trp295-Val321 (Fig. 1a, Extended Data Fig. 1c), the 111-128 loop connecting the P1 pore helix and CAP bearing the extracellular pH sensor, His126[16,17] (Fig. 1a, Extended Data Fig. 1d), and a set of bound lipids (Extended Data Fig. 1e,f).

Structures of the ML335 and ML402 complexes revealed unambiguous density for two activators per channel (Fig. 1b, Extended Data Fig. 2a–e) occupying an L-shaped pocket behind the selectivity filter formed by the P1 pore helix and M4 transmembrane helix intrasubunit interface (Fig. 1c,d). Importantly, contrasting the activated mutant, K_{2P}2.1(TREK-1) G137I[7], K_{2P}2.1(TREK-1)$_{cryst}$ responds to both ML335 and ML402 (Extended Data Fig. 2f–i). The ML335/ML402 binding pocket differs from the TREK antagonist norfluoxetine[6] binding site (Fig. 1e) and is dissimilar to other VGIC superfamily pore domain antagonist sites[18,19] (Extended Data Fig. 3). Thus, the ML335/ML402 site, dubbed the 'K_{2P} modulator pocket', establishes a novel point for VGIC superfamily small molecule modulation.

The K_{2P} modulator pocket comprises a 'P1 face' and an 'M4 face' that form a common set of hydrogen bonds, π-π, and cation-π[20] interactions with ML335 and ML402 (Fig. 2a,b Extended Data Fig. 4a,b). Both compounds adopt an L-shaped conformation enabling their 'upper ring' (ML335 *N*-aryl sulfonamide and ML402 thiophene) and 'lower ring' (ML335 dicholoro-benzyl and ML402 aryl ether) to engage the P1 helix residue Phe134 through face-face and edge-face interactions, respectively (Fig. 2a,b). On the M4 face, the upper and lower rings make a cation-π interaction with Lys271 and edge-face interaction with Trp275, respectively (Fig. 2, Extended Data Fig 2a,b, and 4a,b). The amide groups of both

compounds also make hydrogen bonds with the Ala259 carbonyl on the loop connecting the second selectivity filter. The ML335 sulfonamide forms additional interactions with the Gly260 carbonyl on the same loop, the P1 face Ser131 hydroxyl, the 111-128 loop His126 imidazole nitrogen, and Asn147 on the first selectivity filter (Fig. 2a, Extended Data Fig 4a).

The K_{2P} modulator pocket constitutes a cryptic binding site requiring conformational changes centered around Phe134, Lys271, and Trp275 (Fig. 2c,d, Extended Data Video V1). Without activators, Phe134 and the M4 helix N-terminal end occlude the pocket. These elements move towards the selectivity filter and away from the P1 helix, respectively, to allow access. Lys271 and Trp275 are mobile in the unliganded structure (Extended Data Fig. 5a and 6b), change conformation to form modulator interactions, and together with Phe134 have reduced bound state mobility (Extended Data Fig. 5a–c, and Table 2a). Hence, both compounds act as wedges driven into the selectivity filter supporting structure, a mode reminiscent of other channel modulators[21,22]. Notably, the K_{2P} modulator pocket includes GOF mutation sites, Gly137 and Trp275, affecting all TREK subfamily members[7,8,15,23] (Extended Data Fig. 6b). Together, these observations indicate that the P1/M4 interface is a hub for conformational changes causing TREK subfamily activation and that P1/M4 interface stabilization is central to ML335 and ML402 action.

K_{2P} activator pocket residues that contact the compounds are identical among TREK subfamily members, except for the Lys271 cation-π interaction, and diverge in other K_{2P} subtypes (Extended Data Fig. 4c,d). Comparison with K_{2P}10.1(TREK-2)[6] and K_{2P}4.1(TRAAK)[4,13–15] (Extended Data Fig. 6a, Table 2b) reveals no selectivity filter conformation differences. This structural similarity supports the idea that ML335 and ML402 influence selectivity filter dynamics, similar to inferences from structural studies of P1/M4 interface GOF mutants[15]. There are notable differences in the first two M4 helical turns of the K_{2P} modulator pocket and the conformations of the Phe134 and Trp275 equivalent positions among TREK subfamily structures (Extended Data Fig. 6b–f). Given the varied conformations of these residues in the absence of activators and mobility changes between the unliganded and liganded structures (Extended Data Fig. 5), the main action of the activator appears to be to limit the conformations sampled by P1/M4 interface elements.

The K_{2P}2.1(TREK-1) C-tail senses phospholipid[24,25], phosphorylation[26,27], temperature[7,28], and pressure[27] gating commands and forms a continuous helix with M4 (Fig. 3a). Prior TREK subfamily structures uncovered varied M4 conformations spanning extremes termed ‘up’ and ‘down’[4,6,13–15]. Proposals that the ‘up’[14], ‘down’[15], or both conformations are active [6,23], have been advanced. In all K_{2P}2.1(TREK-1) structures, M4 is ‘up’ (Fig. 1a) and the selectivity filter sites S1–S4 are occupied by potassium ions (Extended Data Fig. 6a). Because both C-tails make lattice contacts (Extended Data Fig. 1g) that can influence M4[13,15], the K_{2P}2.1(TREK-1) structures cannot directly address the controversy regarding M4 status. Nevertheless, the activator-bound selectivity filter is compatible with the ‘up’ M4 conformation.

The C-tail has two faces, an electropositive patch comprising four residues implicated in PIP_2 modulation (Arg297, Lys301, Lys302, and Lys304)[24,25], and a face housing the intracellular proton sensor site, Glu306[29], and inhibitory phosphorylation site, Ser300[26]

(Fig. 3a,b). The channel electrostatic profile shows a second positively charged region at the M1/M2/M4 junction (Fig. 3b) suggesting that the resultant interhelical groove may be a phospholipid binding site.

All three K_{2P}2.1(TREK-1) structures revealed tubular densities at locations different from previous K_{2P} lipid binding sites[4,6,14,15], denoted as lipids L1, L2, and L3 (Fig. 3c, Extended Data Fig. 1e,f). L1 resides at the M2/P2 intersubunit junction (Fig. 3c). L2 and L3 are part of a single phospholipid (Extended Data Fig. 1e,f) and sit in the groove formed by the positively charged M1/M2/M4 intersubunit junction (Fig. 3b and c, Extended Data Fig. 1e,f). The L2/L3 site seems to be a prime point for modulatory lipids, as the positively charged residues that affect PIP_2 responses[24,25] are on the helical face opposite to L2/L3 and M4 conformational changes could affect how these residues interact with regulatory lipid headgroups.

Xenopus oocyte two electrode voltage-clamp measurements show that ML335 and ML402 activate K_{2P}2.1(TREK-1) and K_{2P}10.1(TREK-2) but not K_{2P}4.1(TRAAK) (14.3 ± 2.7 μM, K_{2P}2.1(TREK-1):ML335; 13.7± 7.0 μM, K_{2P}2.1(TREK-1):ML402; 5.2 ± 0.5 μM, K_{2P}10.1(TREK-2):ML335; and 5.9 ± 1.6 μM, K_{2P}10.1(TREK-2):ML402) (Fig. 4a–f, Extended Data Fig. 7a–c). The K_{2P} modulator pocket has a single difference among TREK subfamily members at the cation-π interaction position, K_{2P}2.1(TREK-1) Lys271 (Extended Data Fig. 4c), which is also a lysine in K_{2P}10.1(TREK-2) but a glutamine in K_{2P}4.1(TRAAK). Hence, we asked whether this residue controlled the selective actions of ML335 and ML402. Swapping the Lys271 equivalent between K_{2P}2.1(TREK-1) and K_{2P}4.1(TRAAK) resulted in a clear phenotype reversal for ML335 and M402 activation (Fig. 4c and f, Extended Data Fig. 7d–g). K_{2P}2.1(TREK-1) K271Q was insensitive to ML335 and ML402, whereas K_{2P}4.1(TRAAK) Q258K responded to both with a similar EC_{50} to K_{2P}2.1(TREK-1) (14.3 ± 2.7 μM, K_{2P}2.1(TREK-1):ML335; 16.2 ± 3.0 μM, K_{2P}4.1(TRAAK) Q258K:ML335; 13.7± 7.0 μM, K_{2P}2.1(TREK-1):ML402; 13.6 ± 1.5 μM, K_{2P}4.1(TRAAK) Q258K:ML402) but with a lower magnitude response than K_{2P}2.1(TREK-1). Notably, the effects of TREK subfamily activators arachidonic acid (AA)[27,30], BL-1249[31,32], and ML67-33[11] were unchanged (Extended Data Fig. 7h–k). To probe the cation-π interaction further, we synthesized a ML335 congener, ML335a, in which the aromatic upper ring was replaced with an aliphatic ring (Fig. 4c). ML335a had no effect on K_{2P}2.1(TREK-1) (Fig. 4c), supporting the importance of the cation-π interaction. Together, these data identify the Lys271 cation-π interaction as the origin of ML335/ML402 subtype selectivity and establish that this interaction is essential for activation.

The principal K_{2P} channel gating site is the selectivity filter ‘C-type’ gate[7–10]. This gate is highly sensitive to permeant ions[8,16,17] and is thought to function via ‘flux gating’ whereby outward, but not inward, ion flow stabilizes the active conformation[9]. Physiological K_{2P}2.1(TREK-1) activators, such as AA, PIP_2, and intracellular acidification, shift the channel from outward rectifier mode to an ohmic ‘leak mode’[9]. Because K_{2P} modulator pocket contains architectural elements that support the selectivity and GOF mutant sites that activate the C-type gate[7,8,15], we asked whether P1/M4 interface structural changes caused by ML335, ML402, or GOF mutation impact C-type gate function.

Measurement of K_{2P}2.1(TREK-1) in inside-out patches under conditions that potentiate flux-dependent C-type gate activation (150 mM $K^+_{[out]}$ versus 150 mM $Rb^+_{[in]}$)[9] showed the expected outward rectification (Fig. 4g and k). ML335 and ML402 activate K_{2P}2.1(TREK-1) in HEK293 cells similar to their effects in *Xenopus* oocytes (5.2 ± 0.8 μM and 5.9 ± 1.6 μM for ML335 and ML402, respectively (n≥3)) (Fig. 4g–i, Extended Data Fig. 8a). Compound application essentially eliminated flux-dependent outward rectification (Fig. 4h,i, and k) yielding a rectification coefficient (I_{+100mV}/I_{-100mV}) of ~1. This outcome matches physiological activator effects[9] and establishes that ML335 and ML402 activate the C-type gate. The K_{2P}4.1(TRAAK) GOF mutation G124I reshapes the K_{2P} modulator pocket through structural consequences similar to ML335/ML402, namely an outward M4 movement and repositioning of the K_{2P}2.1(TREK-1) Phe134 equivalent residue[15] (Extended Data Fig. 6f). K_{2P}2.1(TREK-1) G137I and K_{2P}4.1(TRAAK) G124I[7,15] caused a similar mode shift and rectification coefficient change to ML335 and ML402 (Fig. 4j and k, Extended Data Fig. 8b–d) establishing that K_{2P} modulator pocket manipulation by ML335/ML402 binding or mutation directly activates the selectivity filter C-type gate. Together with the compound binding induced mobility reduction of the P1/M4 interface (Extended Data Fig. 5) and lack of K_{2P} selectivity filter structural differences (Extended Data Fig. 6a), our findings strongly support the idea that direct C-type gate activators stimulate function by reducing the dynamics of the selectivity filter and surrounding structure.

The roles of TREK channels in ischemia, pain, analgesia, and anesthetic responses[1] suggests that TREK activators could provide new avenues for neuroprotection and pain control. Many natural TREK regulators are thought to act on the C-tail[7,24–29] and influence the C-type gate through M4 [6–8,15,23] whose movement is targeted by the antagonist norfluoextine[6,23]. In this regard, ML335 and ML402 represent a new K_{2P} modulator class, as they function by binding directly to a pocket at the heart of the channel active site, the C-type gate, rather than influencing the C-tail or M4.

The K_{2P} modulator pocket defines the first VGIC superfamily pore domain small molecule activator site and differs from antagonist sites occupying lateral fenestrations below the selectivity filter[6,18] (Fig. 1e, Extended Data Fig. 3a). Voltage-gated calcium channel antagonists, amlodipine and nifedipine[19], act at an interface similar to the K_{2P} modulator pocket, but at a pore domain outer rim site normally occupied by lipids[19] (Extended Data Fig. 3b). Notably, all of these small molecule sites are found at interfaces that are thought to move during gating[6,18,19], highlighting the potential of channel intersubunit interfaces as small molecule control sites.

Our findings provide a structural basis for understanding K_{2P} C-type gate activation. The K_{2P} modulator pocket in unliganded K_{2P}2.1(TREK-1) displays mobility in key elements that is reduced upon activator engagement (Fig. 4l, Extended Data Figs. 5, 6b–d, and Video V1). Notably, the K_{2P} modulator pocket M4 helix N-terminal end, an important site for channel activation[8] and conduit for transmitting C-tail sensor domain cues to the C-type gate[7,8], adopts a similar position in the ML335 and ML402 K_{2P}2.1(TREK-1) complexes and in K_{2P}4.1(TRAAK) G124I (Extended Data Fig. 6f). As the remainder of M4 is ‘up’ for the K_{2P}2.1(TREK-1) activator complexes, but ‘down’ for K_{2P}4.1(TRAAK) G124I, the data support the idea that M4 position is not the sole determinant of channel state[23]. The

importance of changes in P1/M4 interface dynamics explain how M4 can affect channel function and allow the ‘up’ or ‘down’ conformations to activate the channel[23], as both states could limit the mobility of the P1/M4 interface. Such plasticity may be important for enabling TREK subfamily polymodal modulation. Our findings indicate that under basal conditions, K_{2P}2.1(TREK-1) equilibrates between a resting state having a mobile P1/M4 interface and an activated state in which the mobility of this site is limited. ML335 and ML402 directly stabilize the C-type gate by acting like molecular wedges that reduce P1/M4 interface dynamics (Fig. 4l, Extended Data Fig. 5 and Table 2a) and cause the filter to enter the ‘leak mode’ (Fig. 4h, i), bypassing modulation mechanisms that may involve other channel regions. The K_{2P} modulator pocket properties revealed by our studies raise the possibility that natural processes or native signaling molecules may also target this site.

Opening the cryptic K_{2P} modulator pocket requires small movements of few residues, similar to soluble protein cryptic modulator sites[33]. K_{2P} modulator pocket diversity (Extended Data Fig. 4c,d), the P1/M4 interface susceptibility to GOF mutations[7,8], and demonstration that a single residue therein can define modulator selectivity suggests that this site may be amenable for K_{2P} subtype-selective pharmacology development. As the fundamental pocket architecture is conserved in the VGIC superfamily, similar modulatory mechanisms may exist in other superfamily members where selectivity filter based gating is central. Thus, this site should provide a fertile target for channel modulator discovery.

Methods

No statistical methods were used to predetermine sample size. No randomization or blinding was used.

Construct screening

A set of mutants and deletion constructs of mouse K_{2P}2.1(TREK-1)[1] bearing a C-terminal TEV protease cleavage site and GFP were expressed from a pcDNA3.1 in HEK293 cells and screened for expression level and peak quality using Fluorescence-detection Size Exclusion Chromatography (FSEC)[39–41]. These efforts identified a construct, hereafter called K_{2P}2.1(TREK-1)$_{cryst}$, encompassing residues 21-322 and bearing the following mutations: K84R, Q85E, T86K, I88L, A89R, Q90A, A92P, N95S, S96D, T97Q, N119A, S300A, E306A. The first nine mutations are located on the surface of the CAP domain and greatly increased expression. N119A targets a putative glycosylation site. S300A and E306A are previously studied mutants[7] that improved the biochemical properties of the purified protein. The reduced response of K_{2P}2.1 (TREK-1)$_{cryst}$ to ML335 and ML402 likely results from partial activation of the channel in a cellular context due to the incorporation of the E306A mutation[7,29] and is compatible with the model proposed in Fig. 4l in which basal activity is increased by E306A but can nevertheless be shifted to the C-type gate activated state by activator binding and C-type gate stabilization.

Protein Expression

K_{2P}2.1(TREK-1)$_{cryst}$ bearing a C-terminal green fluorescent protein (GFP) and His_{10} tag was expressed from a previously described *P. pastoris* pPICZ vector[4]. Plasmids were

linearized with *PmeI* and transformed into *P. pastoris* SMD1163H by electroporation. Multi-integration recombinants were selected by plating transformants onto Yeast Extract Peptone Dextrose Sorbitol (YPDS) plates having increasing concentrations of zeocin (1–4 mg ml^{-1}). Expression levels of individual transformants were evaluated by FSEC as previously described[15].

Large-scale expression was carried out in a 7L Bioreactor (Labfors5, Infors HT). First, a 250 ml starting culture was grown in buffered minimal medium (2x YNB, 1% Glycerol, 0.4 mg L^{-1} biotin, 100 mM potassium phosphate, pH 6.0) in shaker flasks for two days at 29°C. Cells were pelleted by centrifugation (3000 x g, 10', 20°C) and used to inoculate the bioreactor. Cells were grown in minimal medium (4% glycerol, 0.93 g L^{-1} $CaSO_4.2H_2O$, 18.2 g L^{-1} K_2SO_4, 14.9 g L^{-1} $MgSO_4.7H_2O$, 9 g L^{-1} $(NH_4)_2SO_4$, 25g L^{-1} Na^+ hexametaphosphate, 4.25ml L^{-1} PTM_1 trace metals stock solution prepared accordingly to standard Invitrogen protocol) until the glycerol in the fermenter was completely metabolized marked by a spike in pO_2 (~24 hours). Fed-batch phase was then initiated by adding a solution of 50% glycerol and 12ml L^{-1} of trace metals at 15%–30% of full pump speed until the wet cell mass reached ~250 g L^{-1} (~24 hours). pO_2 was measured continuously and kept at a minimum of 30%. Feed rate was automatically regulated accordingly. pH was maintained at 5.0 by the addition of a 30% ammonium hydroxide solution.

After the fed-batch phase was completed, cells were then starved to deplete glycerol by stopping the feeder pump until a pO_2 spike appeared. After starvation, the temperature was set to 27°C, and the induction was initiated with addition of methanol in three steps: (1) Initially, the methanol concentration was kept at 0.1% for 2 h in order to adapt the cells. (2) Methanol concentration was then increased to 0.3% for 3h, and (3) methanol was then increased to 0.5% and expression continued for ~48–60 hours. Cells were then pelleted by centrifugation (6000 x g,1h, 4°C), snap frozen in liquid nitrogen, and stored at −80°C.

Protein Purification

In a typical preparation, 50 g of cells were broken by cryo-milling (Retsch model MM400) in liquid nitrogen (5 x 3 min, 25 Hz). All subsequent purification was carried out at 4° C. Cell powder was added at a ratio of 1g cell powder:3ml lysis buffer (200 mM KCl, 21 mM OGNG [Octyl Glucose Neopentyl Glycol, Anatrace], 30 mM HTG [n-heptyl-β-D-thioglucopyranoside, Anatrace], 0.1% CHS, 0.1 mg mL^{-1} DNAse 1 mM PMSF, 100 mM Tris-Cl, pH 8.2). Membranes were extracted for 3 hours with gentle stirring followed by centrifugation at (100000 x g, 45' at 4°C).

Solubilized proteins were purified by affinity chromatography using batch purification. Anti-GFP nanobodies were conjugated with CNBr Sepharose beads (GE Healthcare, #17-0430-02) according to reference [42]. The resin was added to the cleared supernatant at a ratio of 1 ml of resin per 10 g of cell powder and incubated at 4°C for 3h with gentle shaking. Resin was collected into a column and washed with 10 column volumes (CV) of buffer A (200 mM KCl, 10 mM OGNG, 15 mM HTG, 0.018% CHS, 50 mM Tris-Cl, pH8.0) followed by a second wash step using 10 CV of buffer B containing (200 mM KCl, 5 mM OGNG, 15 mM HTG, 0.018% CHS, 50 mM Tris-Cl, pH8.0). The resin was then washed with additional 10 CV of buffer C (200 mM KCl, 3.85 mM OGNG, 15 mM HTG, 0.0156%

CHS, 50 mM Tris-Cl, pH 8.0). On column cleavage of the affinity tag was achieved by incubating the resin with buffer C supplemented to contain 350 mM KCl, 1 mM EDTA, and 3C protease[43] at ratio of 50:1 resin volume:protease volume. The resin was incubated overnight at 4°C. Cleaved sample was collected and the resin washed with 2 CV of SEC buffer (200 mM KCl, 2.1 mM OGNG, 15 mM HTG, 0.012% CHS, 20 mM Tris-Cl, pH 8.0). Purified sample was concentrated and applied to a Superdex 200 column equilibrated in SEC buffer.

Crystallization and Refinement

Purified K_{2P}2.1(TREK-1)$_{cryst}$ was concentrated to 6 mg ml^{-1} by centrifugation (Amicon® Ultra-15, 50 kDa molecular mass cutoff; Millipore) and crystallized by hanging-drop vapor diffusion at 4°C using a mixture of 0.2 µl of protein and 0.1 µl of precipitant over 100 µl of reservoir containing 20–25% PEG400, 200 mM KCl, 100 mM HEPES pH 8.0, 1 mM $CdCl_2$. Crystals appeared in 12 hours and grew to full size (200µm-300µm) in about a week. Crystals were cryoprotected with buffer D (200 mM KCl, 0.2% OGNG, 15 mM HTG, 0.02% CHS, 100 mM HEPES pH 8.0,1 mM $CdCl_2$) with 5% step increase of PEG400 up to a final concentration of 38% and flash frozen in liquid nitrogen.

K_{2P}2.1(TREK-1)$_{cryst}$ ML335 and ML402 complex crystals grew in the same conditions as K_{2P}2.1(TREK-1)$_{cryst}$, but the protein was incubated for at least 1h with 2.5mM of activator before setting the crystal plates. ML335 and ML402 are insoluble in aqueous solutions, so they were dissolved in 100% DMSO at a concentration of 500 mM. Then each compound was diluted 1:100 in SEC buffer to 5 mM concentration, giving a milky solution. This solution was mixed 1:1 to K_{2P}2.1(TREK-1)$_{cryst}$ previously concentrated to 12 mg ml^{-1}. The K_{2P}2.1(TREK-1)$_{crys}$ /ML402 mixture resulted in a clear solution, while the mixture with ML335 was slightly milky. The samples were briefly centrifuged in a table top centrifuge (10.000 x g) to remove any insoluble material before setting the crystal plates.

Datasets for K_{2P}2.1(TREK-1), K_{2P}2.1(TREK-1):ML335, and K_{2P}2.1(TREK-1):ML402 were collected at 100 K using synchrotron radiation at ALS Beamline 8.3.1 Berkeley, CA and APS GM/CAT beamline 23-IDB/D Chicago, IL using wavelengths of 1.1159Å and 1.0332Å, respectively, processed with XDS[44], scaled and merged with Aimless[45]. Final resolution cutoff was 3.1Å and 3.0 Å and 2.8 Å for K_{2P}2.1(TREK-1)$_{cryst}$, K_{2P}2.1(TREK-1)$_{cryst}$:ML335, and K_{2P}2.1(TREK-1)$_{cryst}$:ML402, respectively, using the $CC_{1/2}$ criterion[46,47]. Structures were solved by molecular replacement using the K_{2P}4.1(TRAAK) G124I structure (PDB 4RUE)[15] as search model. Several cycles of manual rebuilding, using COOT[48], and refinement using REFMAC5[49] and PHENIX[50] were carried out to improve the electron density map. Two-fold local medium NCS restraints were employed during refinement for residues 28-103, 110-158 and 194-260.

K_{2P}2.1(TREK-1), K_{2P}2.1(TREK-1):ML335, and K_{2P}2.1(TREK-1):ML402 structures have, respectively, 95.2%/0.4%, 92.0%/0.5% and 95.7%/0.4% residues in favored regions/outliers of the Ramachandran plot as assessed by Molprobity[51].

Electrophysiology

Patch-clamp electrophysiology—mouse K_{2P}2.1(TREK-1), human K_{2P}4.1(TRAAK), and mutants were expressed from a previously described pIRES2-EGFP vector[8,11] in HEK 293T cells (ATTC). 70% confluent cells were transfected (in 35 mm diameter wells) with LipofectAMINE™ 2000 (Invitrogen, Carlsbad, CA, USA) for 6 hours, and plated onto coverslips coated with Matrigel (BD Biosciences, San Diego, CA, USA).

Effects of ML335, ML402, and arachidonic acid on K_{2P}2.1(TREK-1) current at 0 mV were measured by whole cell patch-clamp experiments 24 hours after transfection. Acquisition and analysis were performed using pCLAMP9 and an Axopatch 200B amplifier (Molecular Devices, Sunnyvale, CA, USA). Pipette resistance ranged from 1 to 1.5 MΩ. Pipette solution contained the following, in millimolar: 145, KCl; 3, $MgCl_2$; 5, EGTA and 20, HEPES (pH 7.2 with KOH). Bath solution contained the following, in millimolar: 145, NaCl; 5, KCl; 1, $CaCl_2$; 3, $MgCl_2$; 20, HEPES (pH 7.4 with NaOH). K_{2P}2 (TREK-1) currents were elicited by a 1 second ramp from –100 to +50 mV from a –80 mV holding potential. After stabilization of the basal current, ML335 and ML402 were perfused at 200 ml hr^{-1} until potentiation was stably reached.

Voltage-dependent activation of K_{2P}2.1(TREK-1) was recorded on excised patches in inside-out configuration (50kHz sampling) in the absence and presence of 5 μM ML335 or ML402. Pipette solution contained the following, in millimolar: 150 KCl; 3.6 $CaCl_2$; 10 HEPES (pH 7.4 with KOH). Bath solution contained the following, in millimolar: 150 RbCl; 2 EGTA and 10 HEPES (pH 7.4 with RbOH), and was continuously perfused at 200 ml hr^{-1} during the experiment. TREK-1 currents were elicited by a voltage step protocol from −100mV to +100mV, from a –80 mV holding potential (or −10mV for K_{2P}2.1(TREK-1) G137I and K_{2P}4.1(TRAAK) G124I in presence of the compounds after exposing the patch to the compound for 30 s at −80 mV). Data were analyzed using Clampfit 9 and Origin 7.

Two Electrode Voltage Clamp Electrophysiology—Two electrode voltage clamp recordings were performed on defolliculated stage V–VI *Xenopus laevis* oocytes 24–48 h after microinjection with 0.15–5 ng cRNA. Oocytes were impaled with borosilicate recording microelectrodes (0.3–3.0MΩ resistance) backfilled with 3M KCl. Recording solution (96 mM NaCl, 2 mM KCl, 1.8 mM $CaCl_2$, and 2.0 mM $MgCl_2$, buffered with 5 mM HEPES, pH 7.4) was perfused at a rate of 3 ml min^{-1}.

Currents were evoked from a −80mV holding potential followed by a 300 ms ramp from −150 mV to +50 mV. Data were acquired using a GeneClamp 500B amplifier (MDS Analytical Technologies) controlled by pClamp software (Molecular Devices), and digitized at 1 kHz using Digidata 1332A digitizer (MDS Analytical Technologies).

Dose-response experiments were carried by first preparing a DMSO stock solution of each activator at a concentration of 100 mM. Due to the low solubility of the compounds the highest tested concentrations in recording solution were 100 μM and 80 μM for ML335 and ML402, respectively (final concentration of DMSO was 0.2%). Other concentrations were prepared by serial dilutions of the 100 μM solution in recording buffer supplemented with 0.1% DMSO.

Xenopus oocytes were collected incompliance with ethical regulations specified by the UCSF Institutional Animal Care and Use Committee protocol AN129690.

Synthetic chemistry—Detailed descriptions of synthesis routes and characterization of ML335, ML335a, and ML402 are found in the supplementary material.

Extended Data

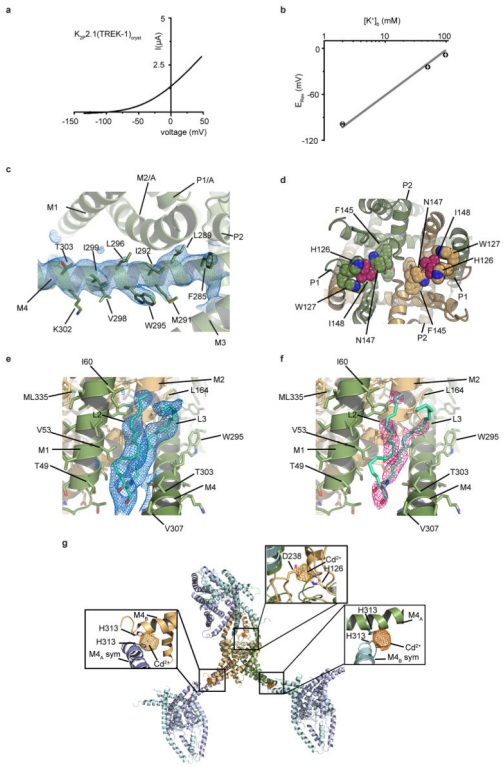

Extended Data Figure 1. $K_{2P}2.1(TREK\text{-}1)_{cryst}$ function and structure

a, Exemplar recording from $K_{2P}2.1(TREK\text{-}1)_{cryst}$ expressed in *Xenopus* oocytes. Current was elicited from a −80mV holding potential followed by a 500 ms ramp from −150 mV to +50 mV. **b**, $K_{2P}2.1(TREK\text{-}1)_{cryst}$ potassium selectivity recorded in *Xenopus* oocytes in K^+/N-methyl-D-glucamine solutions (98.0 mM total) at pH_o= 7.4. Data represent mean ± SEM (n= 4). Dashed gray line represents Nernst equation $E_{rev}=RT/F*\log([K^+]_o/[K^+]_i)$, where R and F have their usual thermodynamic meanings, z is equal to 1, and T=23°C, assuming $[K^+]_I$ = 108.6 mM[34]. **c,** Exemplar $2F_o\text{-}F_c$ electron density (1.0 σ) for the C-tail region of $K_{2P}2.1(TREK\text{-}1)_{cryst}$. Select residues and channel elements are indicated. **d,** Extracellular view of $K_{2P}2.1(TREK\text{-}1)_{cryst}$ showing environment of His126 and Ile148 (raspberry). Select residues are labeled. The extracellular proton sensor His126[16,17] is supported by a highly conserved residue, Trp127, and contacts a gain-of-function (GOF) mutant site, Ile148[8], that interacts with the selectivity filter residue Asn147. This network of physical interactions indicates how changes at His126[16,17] or Ile148[8] could affect the C-type gate. **e,** and **f,** Exemplar L2/L3 lipid electron density for $K_{2P}2.1(TREK\text{-}1)$:ML335. **e,** 2Fo-Fc, (blue, 1.0 σ) and **f,** $F_o\text{-}F_c$, (hotpink, 3.0 σ). Chains are colored smudge and light orange.

Channel elements and select residues are labeled. **g,** Crystal lattice packing for $K_{2P}2.1(TREK\text{-}1)_{cryst}$ showing that the C-tail makes lattice interactions stabilized by a cadmium ion coordinated between His313 of adjacent symmetry mates. Asymmetric unit is colored smudge (chain A) and light orange (chain B). Symmetry related channels are shown in slate (chain A) and cyan (chain B). Insets show the anomalous difference map (5.0σ) and locations of Cd^{2+} ions and their ligands.

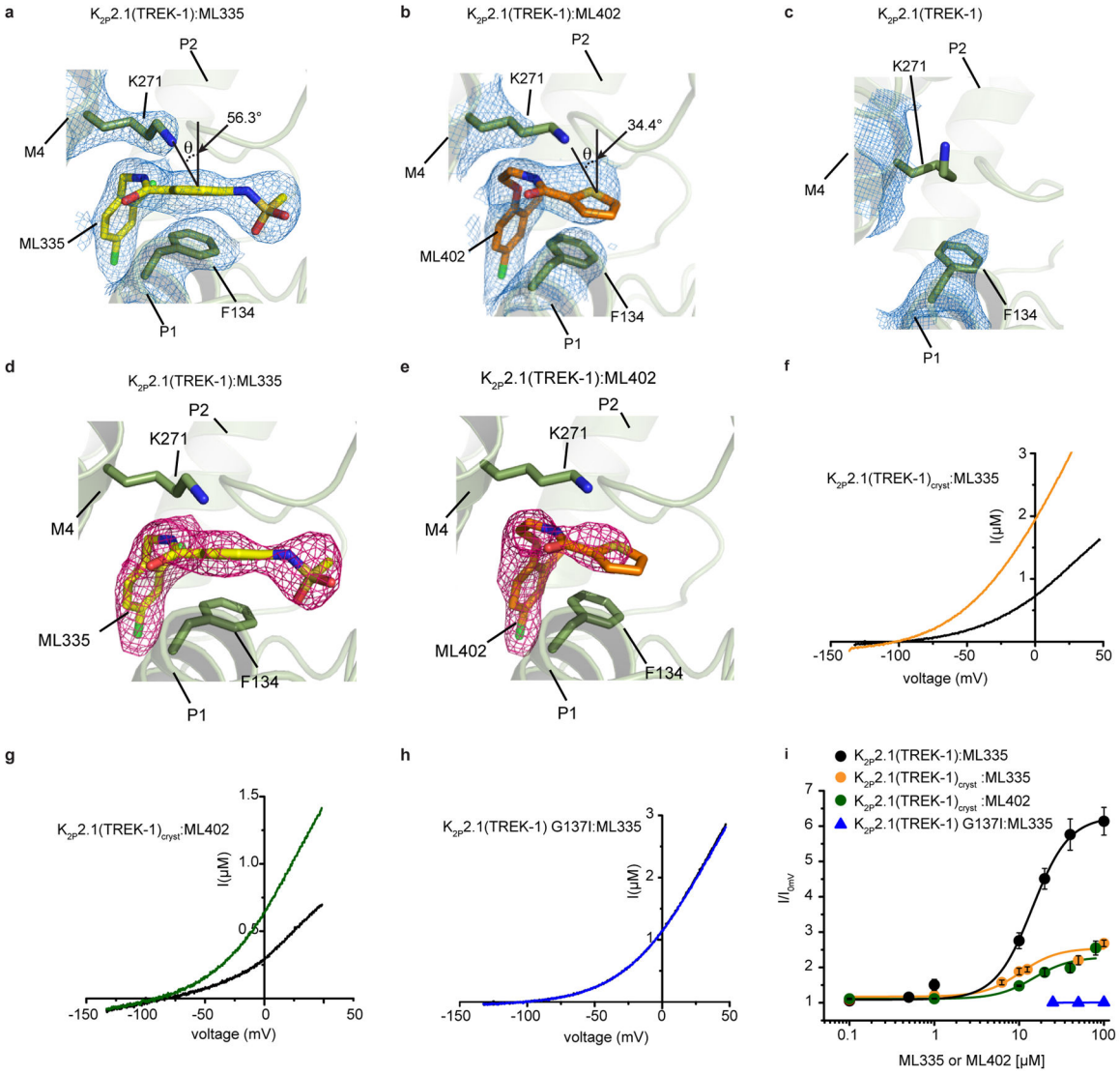

Extended Data Figure 2. $K_{2P}2.1(TREK\text{-}1)_{cryst}$ modulator binding pocket densities and $K_{2P}2.1(TREK\text{-}1)_{cryst}$ functional properties

a–e, Exemplar electron densities for the modulator binding pockets. a–c, $2F_o\text{-}F_c$ densities (blue) for a, $K_{2P}2.1(TREK\text{-}1)$:ML335 (1.5 σ), b, $K_{2P}2.1(TREK\text{-}1)$:ML402 (1.0 σ), and c, K_{2P} 2.1(TREK-1) (1.0 σ). Offset angle for the cation-π interactions for Lys271:ML335 and Lys271:ML402 is shown and adopts an oblique geometry common to cation-π interactions[35,36]. d, and e, $F_o\text{-}F_c$ densities (hotpink, 3.0 σ) for d, $K_{2P}2.1(TREK\text{-}1)$:ML335 and e, $K_{2P}2.1(TREK\text{-}1)$:ML402. Final models are shown in all panels and select residues are

shown and labeled. f–h, Exemplar current traces for f, K_{2P}2.1 (TREK-1)$_{cryst}$ (black) with 40 μM ML335 (yellow orange), g, K_{2P}2.1 (TREK-1)$_{cryst}$ (black) with 80 μM ML402 (green), and h, K_{2P}2.1 (TREK-1) G137I (black) with 80 μM ML335 (blue). i, Dose response curves for K_{2P}2.1(TREK-1):ML335 (black), EC_{50}=14.3 ± 2.7 μM (n≥5); K_{2P}2.1 (TREK-1)$_{cryst}$:ML335, EC_{50} = 10.5 ± 2.7 μM (n≥3) (yellow orange) K_{2P}2.1 (TREK-1)$_{cryst}$:ML402, EC_{50} = 14.9 ± 1.6 μM (n≥3); and K_{2P}2.1(TREK-1) G137I:ML335 (blue).

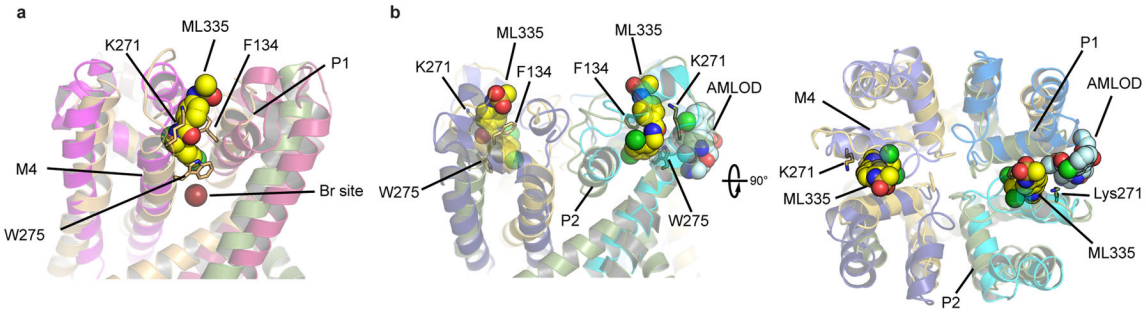

Extended Data Figure 3. Comparison of K_{2P} modulator and VGIC antagonist sites

a, Superposition of the K_{2P}2.1(TREK-1):ML335 complex (smudge and light orange) with the BacNa$_V$ 'pore-only' Na$_V$Ms structure[18] (magenta and warm pink). Bromine site (Br) from labeled sodium channel antagonists is shown as a firebrick sphere. **b,** Superposition of the pore domains of the K_{2P}2.1(TREK-1):ML335 complex (smudge and light orange) with the pore domain of the BacNa$_V$ Ca$_V$Ab (5KMD) bound to the inhibitor amlodipine (AMLOD)[19], a site normally occupied by lipid[19,37]. Select residues of the K_{2P} modulator pocket are shown as sticks and are labeled. Ca$_V$Ab subunits are colored cyan, marine, slate, and dark blue. ML335 (yellow) and amlodipine (cyan) are shown in space filling representation.

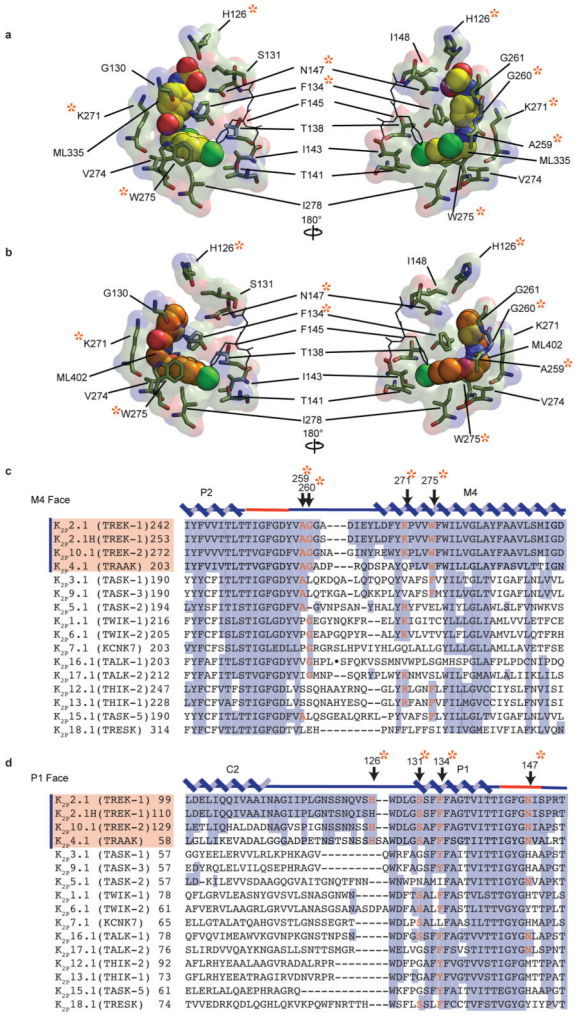

Extended Data Figure 4. K_{2P} modulator pocket structure and conservation

Details of **a**, ML335, and **b**, ML402 interactions with K_{2P}2.1(TREK-1). **c** and **d**, Representative K_{2P} channel sequence comparisons for the **c**, M4 face and **d**, P1 face. Purple bar and orange shading on sequence identifiers denotes the thermo- and mechanosensitive K_{2P}2.1(TREK-1) subfamily. Protein secondary structure is marked above the sequences. Selectivity filter region is in red. Residues involved in direct interactions with ML335 and ML402 are orange and marked with an orange asterisk. Conserved positions are highlighted. K_{2P}2.1(TREK-1) is the mouse protein used for this study. K_{2P}2.1H(TREK-1) is the human homolog. All other K_{2P} sequences are human origin. Sequences and identifiers are as follows: K_{2P}2.1(TREK-1) NP_034737.2; K_{2P}2.1H(TREK-1), NP_001017424.1; K_{2P}10.1(TREK-2), NP_612190.1; K_{2P}4.1(TRAAK), NP_001304019.1; K_{2P}3.1(TASK-1), NP_002237.1; K_{2P}9.1(TASK-3), NP_001269463.1; K_{2P}5.1(TASK-2), NP_003731.1; K_{2P}1.1(TWIK-1), NP_002236.103812.2; K_{2P}6.1(TWIK-2), NP_004823.1; K_{2P}7.1(KCNK7), AAI03812.2; K_{2P}16.1(TALK-1), NP_001128577.1; K_{2P}17.1(TALK-2), NP_113648.2; K_{2P}12.1(THIK-2), NP_071338.1; K_{2P}12.1(THIK-1), NP_071337.2; K_{2P}15.1(TASK-5), NP_071753.2; and K_{2P}18.1(TRESK), NP_862823.1. '●' in

$K_{2P}16.1$(TALK-1) sequence in '**c**' denotes the following, non-conserved sequence that was removed to avoid a long alignment gap: NFITPSGLLPSQEPFQTPHGKPESQQIP.

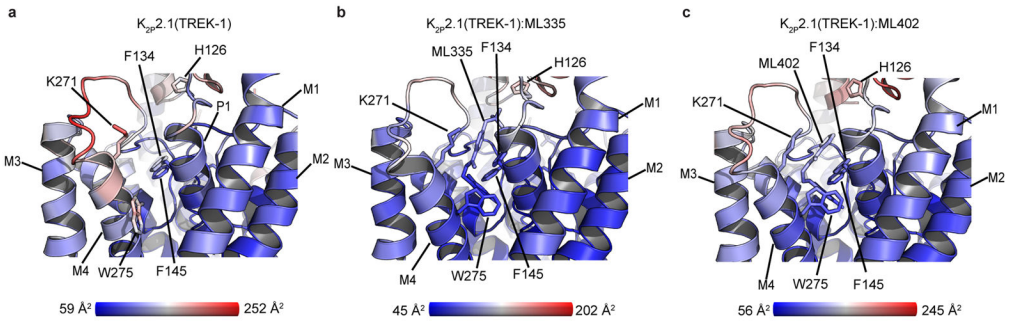

Extended Data Figure 5. K_{2P} structure comparisons

K_{2P} modulator pocket views colored by B-factor for **a,** $K_{2P}2.1$(TREK-1), **b,** $K_{2P}2.1$(TREK-1):ML335**,** and **c,** $K_{2P}2.1$(TREK-1):ML402. Bars show B-factor scale.

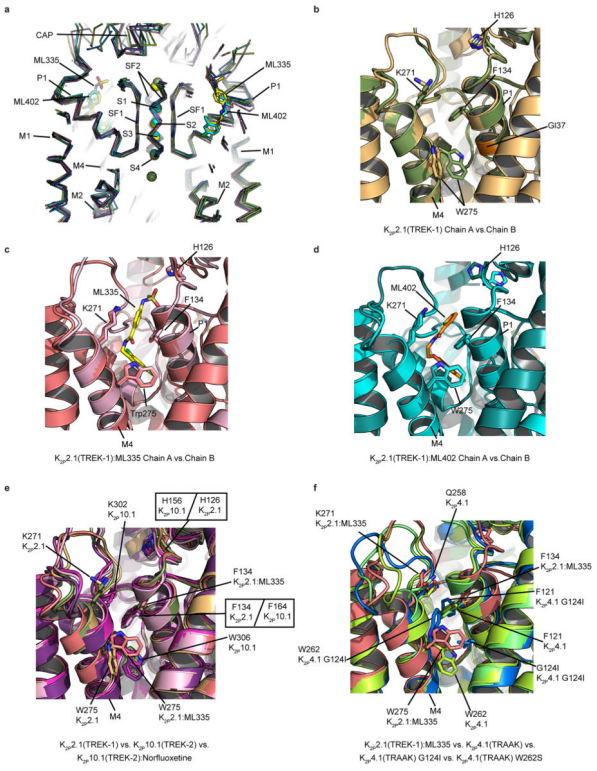

Extended Data Figure 6. K_{2P} structure comparisons

a, Backbone atom superposition of $K_{2P}2.1$(TREK-1) (smudge, up), $K_{2P}2.1$(TREK-1):ML335 (yellow, up), $K_{2P}2.1$(TREK-1):ML402 (cyan, up), $K_{2P}10.1$(TREK-2) (4BW5) (pink, up)[6], $K_{2P}10.1$(TREK-2) (4XDJ) (magenta, down)[6], $K_{2P}10.1$(TREK-2):Norfluoxetine (4XDK)(violet purple, down)[6], $K_{2P}4.1$(TRAAK) (4I9W) (limon, up)[13], $K_{2P}4.1$(TRAAK) G124I (4RUE) (marine, down)[15], and $K_{2P}4.1$(TRAAK) W262S (4RUF) (lime, down)[15]. 'up' or 'down' denotes M4 conformation. Selectivity filter

ions for K_{2P}2.1(TREK-1) (smudge), K_{2P}2.1(TREK-1):ML335 (yellow), and K_{2P}2.1(TREK-1):ML402 (cyan) are shown as spheres. ML335 and ML402 are shown in sticks. Select channel elements are labeled. **b–e,** Superposition showing **b,** K_{2P}2.1(TREK-1) chain A (smudge) and chain B (light orange). Sites of GOF mutations, G137I (orange)[7], and Trp275[8], are indicated. **c,** K_{2P}2.1(TREK-1):ML335 chain A (pink) and chain B (deep salmon), **d,** K_{2P}2.1(TREK-1):ML402 chain A (cyan) and chain B (deep teal). **e,** K_{2P}2.1(TREK-1) chain A (smudge) and chain B (light orange), K_{2P}10.1(TREK-2) (4BW5) (pink)[6], K_{2P}10.1(TREK-2) (4XDJ) (magenta)[6], K_{2P}10.1(TREK-2):Norfluoxetine (4XDK) (violet purple)[6]. **f,** K_{2P}2.1(TREK-1):ML335 (deep salmon), K_{2P}4.1(TRAAK) (4I9W) (limon)[13], K_{2P}4.1(TRAAK) G124I (4RUE) (marine)[15], K_{2P}4.1(TRAAK) W262S (4RUF) (lime)[15]. G124I from K_{2P}4.1(TRAAK) G124I[15] is shown in sticks. In **b–f**, Phe134, His126, Lys271, Trp275, their equivalents in K_{2P}10.1(TREK-2), K_{2P}4.1(TRAAK), and K_{2P}4.1(TRAAK) G124I, are shown in sticks. ML335, **'c'**, and ML402, **'d'**, are shown as sticks.

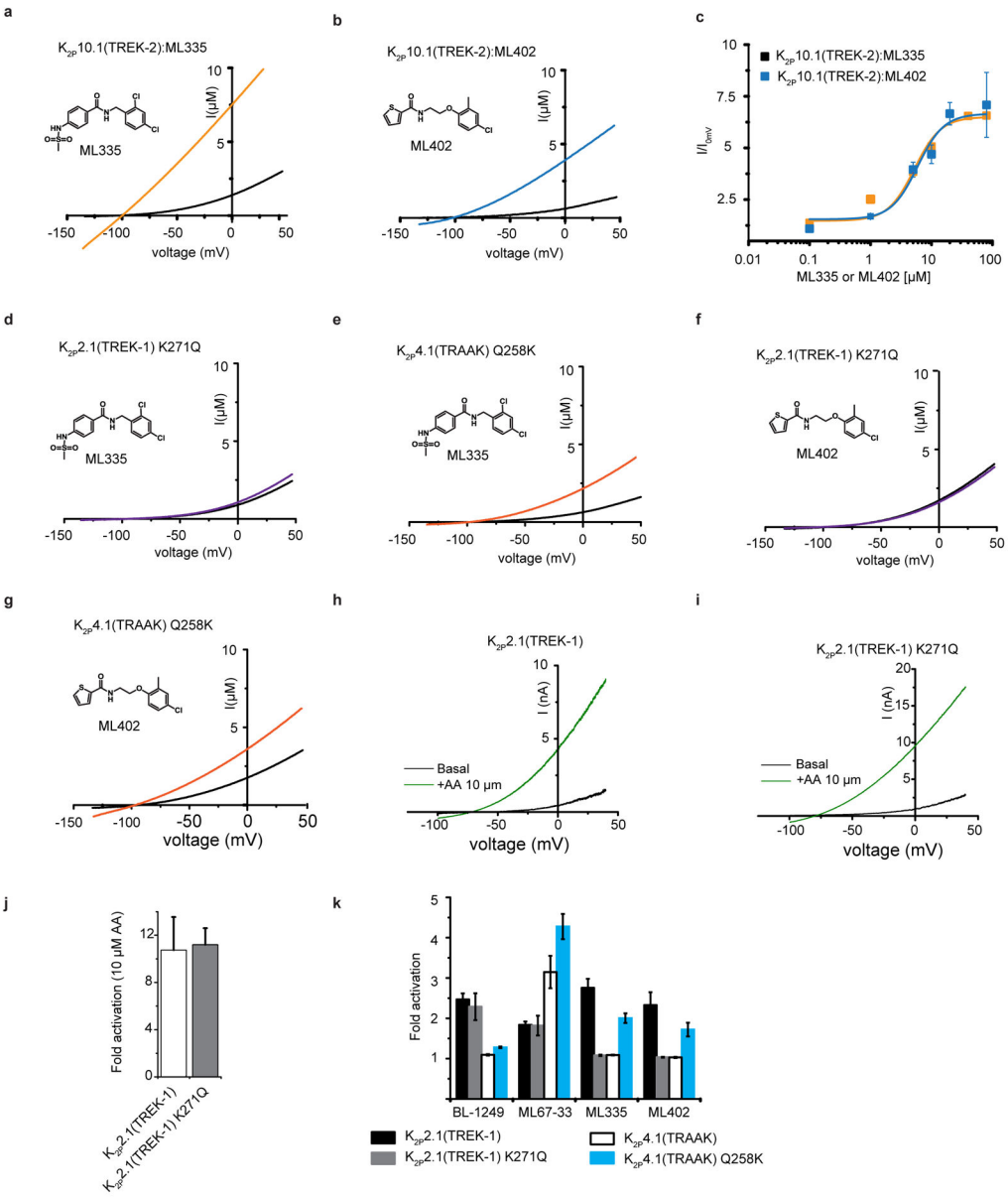

Extended Data Figure 7. K_{2P} activator responses

Exemplar current traces for **a,** K_{2P}10.1(TREK-2) (black) with 20 μM ML335 (yellow orange) and **b,** K_{2P}10.1(TREK-2) (black) with 20 μM ML402 (cyan). **c,** Dose response curves for K_{2P}10.1(TREK-2) with ML335 (EC_{50} = 5.2 ± 0.5 μM (n>3)) (yellow orange) and ML402 (EC_{50} = 5.9 ± 1.6 μM (n≥4)(cyan). Exemplar current traces for **d,** K_{2P}2.1(TREK-1) K271Q (black) and with 20 μM ML335 (purple). **e,** K_{2P}4.1(TREK-1) Q258K (black) and with 50 μM ML335 (orange). **f,** K_{2P}2.1(TREK-1) K271Q (black) and with 50 μM ML402 (purple). **g,** K_{2P}4.1(TREK-1) Q258K (black) and with 50 μM ML402 (orange). Currents were evoked from *Xenopus* oocytes expressing the indicated channels from a −80 mV holding potential followed by a 500 ms ramp from −150 mV to +50 mV. Compound structures are shown. **h,** and **i,** Exemplar current traces for HEK293 cell inside-out patches expressing **h,** K_{2P}2.1(TREK-1) and **i,** K_{2P}2.1(TREK-1) K271Q to stimulation by 10 μM

arachidonic acid (AA) (green). **j,** Current potentiation measured in HEK cells at 0 mV in response to 10μM AA for K_{2P}2.1(TREK-1) (n=5) and K_{2P}2.1(TREK-1) K271Q (n=4). **k,** Current potentiation measured in *Xenopus* oocytes at 0 mV for K_{2P}4.1(TRAAK) (white), K_{2P}2.1(TREK-1) (black), K_{2P}4.1(TRAAK) Q258K (cyan) and K_{2P}2.1(TREK-1) K271Q (gray) in response to 10 μM BL-1249, 30 μM ML67-33, and 20 μM ML335. For all experiments (n≥4). Data are mean ± SEM.

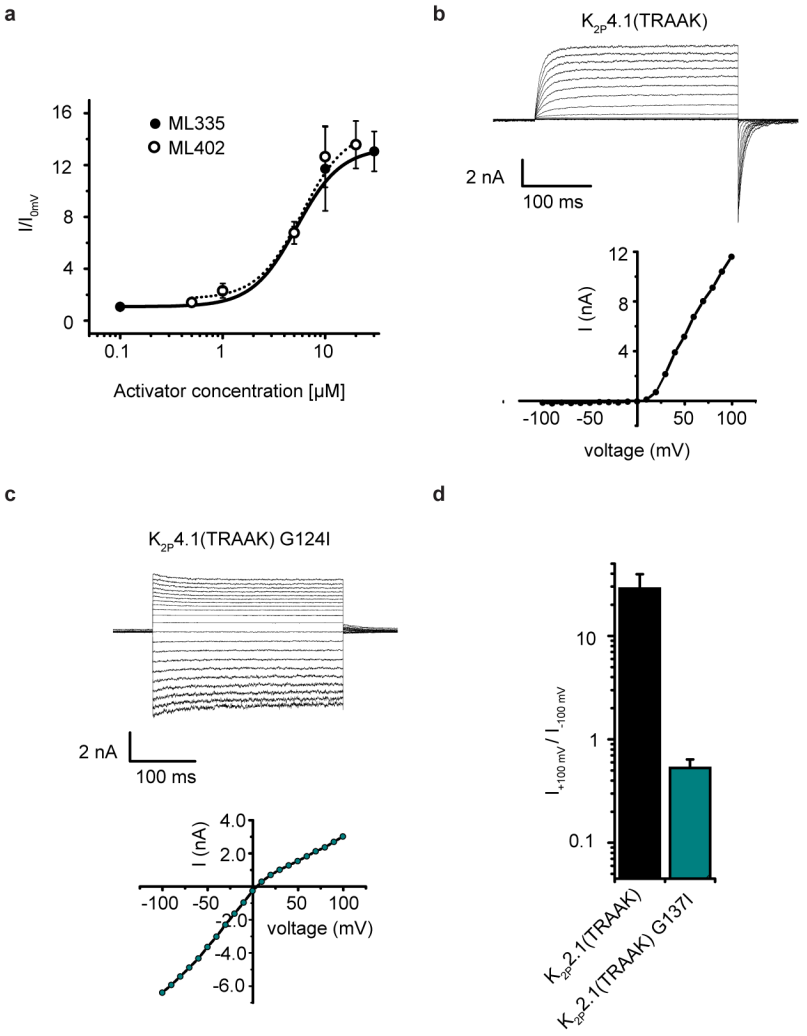

Extended Data Figure 8. K_{2P} channel patch clamp recordings

a, Dose response for K_{2P}2.1(TREK-1) to ML335 (black circles) and ML402 (open circles) measured in HEK293 cells by whole cell patch clamp. EC_{50} values are 5.2 ± 0.8 μM and 5.9 ± 1.6 μM for ML335 and ML402, respectively (n≥3). **b,** and **c,** Representative current traces and voltage-current relationship from HEK293 inside-out patches for expressing **b,** K_{2P}4.1(TRAAK) and **c,** K_{2P}4.1(TRAAK) G124I elicited by a 350 ms-voltage step protocol from −100 mV to +100 mV in 150 mM $K^+_{[out]}$/150 mM $Rb^+_{[in]}$. **d,** Rectification coefficients (I_{+100mV}/I_{-100mV}) calculated from n≥3 current recordings obtained from the same conditions in '**b**' and '**c**'.

Extended data Table 1

Data collection and refinement statistics

	K_{2p}2.1 (TREK-1) (5VK5)	K_{2p}2.1 (TREK-1): ML335 (5VKN)	K_{2p}2.1 (TREK-1):ML402 (5VKP)
Data collection			
Space group	$P2_12_12_1$	$P2_12_12_1$	$P2_12_12_1$
Cell dimensions			
a, *b*, *c* (Å)	66.72/120.42/126.44	67.07/119.39/128.18	67.09/119.56/127.21
α, *β*, *γ* (°)	90.0/90.0/90.0	90.0/90.0/90.0	90.0/90.0/90.0
Resolution (Å)	87.2 – 3.10 (3.21 – 3.10)	87.4 – 3.0 (3.11 – 3.0)	87.1 – 2.8 (2.99 – 2.8)
R_{sym} (%)	10.38 (>100%)	23.7 (>100%)	14.2 (>100%)
$I/\sigma(I)$	13.35 (0.3)	9.78 (0.66)	11.13 (0.37)
$CC_{1/2}$	0.999 (0.065)	0.998 (0.171)	0.999 (0.108)
Completeness (%)	97.0 (100.0)	97.0 (100.0)	98.0 (100.0)
Redundancy	6.0 (6.2)	12.9 (13.3)	12.8 (13.6)
Refinement			
Resolution (Å)	15.0 – 3.10 (3.21 – 3.10)	15.0 – 3.0 (3.11 – 3.0)	15.0 – 2.8 (2.99 – 2.8)
No. reflections	18506	20686	25882
R_{work}/R_{free}	26.1/31.4	25.8/28.3	26.9/31.4
No. atoms			
Protein	4289	4357	4328
Ligand/ion	74	200	174
K^+	6	6	6
Cd^{2+}	3	3	1
Lipid	65	191	167
ML335 or ML402			
Water	0	0	0
B factors			
Protein	154.6	107.4	147.7
Ligand/ion	168.7	96.5	131.0
Water	n/a	n/a	n/a
R.m.s. deviations			
Bond lengths (Å)	0.002	0.006	0.002
Bond angles (°)	0.480	0.685	0.483

[a] Values in parentheses are for highest-resolution shell.

[b] each dataset was derived from a single crystal

Extended data Table 2

K_{2P}2.1(TREK-1) B-factor and structure comparisions a, B-factor comparisons. Selectivity filter residue B-factors are below the average channel core B-factor in both the K_{2P}2.1(TREK-1) and modulator bound structures. Modulator pocket residue B-factors drop relative to the average B-factor in both the ML335 and ML402 complexes, indicating that modulator binding reduces the mobility of these residues. The structures are determined in ~200 mM potassium, a concentration that is expected to stabilize the conformation of the selectivity filter (cf. Ref. [38]) and that could mask mobility changes. Average B-factor is calculated using the channel core elements on both chains: M1 (residues 47-65), P1 through common part of M2 (residues 127-188), common part of M3 through common part M4 (residues 210-300). The selectivity filter was included in the calculation. Blue and red values are >10% below or above the average B-factor, respectively. **b,** K_{2P} channel structure comparisons. RMSDs are calculated using the following K_{2P}2.1(TREK-1) (5VK5) Chain A and Chain B elements: (Δ*CAP*, Δ*M4*) M1 through CAP (residues 47-69), P1 through common part of M4 (residues 127-281). *Channel core (*Δ*CAP,* Δ*M2,* Δ*M4*) M1 (residues 47-65), P1 through common part of M2 (residues 127-188), common part of M3 through common part M4 (residues 210-300). The selectivity filter was included in the calculation. For the non-domain-swapped K_{2P}4.1(TRAAK)(3UM7), residues 47-69 of chain A were compared to equivalent chain B residues.

Extended Data Table 2a | B-factor comparisons for K_{2P}2.1(TREK-1) and modulator complexes

		B-factor (Å^2)		
Location	**Residue**	**K_{2P}2.1(TREK-1)**	**K_{2P}2.1(TREK-1):ML335**	**K_{2P}2.1(TREK-1):ML402**
Selectivity filter	Gly144			
	Phe145			
	Gly146		76.5	127.4
Modulator pocket	Phe134	139.3		
	Lys271		83.0	116.1
	Trp275			
Channel core		132.4	83.5	118.8

Extended Data Table 2b. Structural comparisons with K_{2p}2.1 (TREK-1)

PDB code	**K_{2p}**	**Cα RMSD (Å) (ΔCAP, ΔM4)**	**Cα RMSD(Å) Channel core (ΔCAP, ΔM2, ΔM4)**
5VKN	K_{2p} 2.1(TREK-1):ML335	0.443	0.388
5VKP	K_{2p} 2.1(TREK-1):ML402	0.462	0.426
4XDK	K_{2p} 10.1 (TREK-2):Norfluoxetine	1.976	1.317
4BW5	K_{2p} 10.1(TREK-2):M4 up	1.054	0.918
4XDJ	K_{2p} 10.1(TREK-2):M4 down	1.790	1.331
419W	K_{2p} 4.1(TRAAK)	1.176	1.141
3UM7	K_{2p} 4.1(TRAAK) (no domain swap)	1.468	1.390
4RUF	K_{2p} 4.1(TRAAK) W262S	1.351	1.288
4RUE	K_{2p} 4.1(TRAAK) G124I	1.466	1.490

Extended Data Table 2b. Structural comparisons with K_{2p}2.1 (TREK-1)

PDB code	K_{2p}	Cα RMSD (Å) (ΔCAP, ΔM4)	Cα RMSD(Å) Channel core (ΔCAP, ΔM2, ΔM4)
4WFF	K_{2p} 4.1(TRAAK) M4 down	1.155	1.217
4WFE	K_{2p} 4.1(TRAAK) M4 up	1.149	1.023

Supplementary Material

Refer to Web version on PubMed Central for supplementary material.

Acknowledgments

We thank K. Brejc, S. Capponi, M. Grabe, L. Jan, for comments, and A. Renslo for comments and synthesis advice. This work was supported by grants R01-MH093603 to D.L.M., and to M.L. and C.A. from the American Heart Association.

References

1. Feliciangeli S, Chatelain FC, Bichet D, Lesage F. The family of K channels: salient structural and functional properties. J Physiol. 2014
2. Devilliers M, et al. Activation of TREK-1 by morphine results in analgesia without adverse side effects. Nat Commun. 2013; 4:2941. [PubMed: 24346231]
3. Vivier D, et al. Development of the first Two-Pore Domain Potassium Channel TREK-1 (TWIK-Related K+ Channel 1)-selective agonist possessing in vivo anti-nociceptive activity. Journal of medicinal chemistry. 2017
4. Brohawn SG, del Marmol J, MacKinnon R. Crystal structure of the human K2P TRAAK, a lipid- and mechano-sensitive K+ ion channel. Science. 2012; 335:436–441. 335/6067/436 [pii]. DOI: 10.1126/science.1213808 [PubMed: 22282805]
5. Miller AN, Long SB. Crystal structure of the human two-pore domain potassium channel K2P1. Science. 2012; 335:432–436. 335/6067/432 [pii]. DOI: 10.1126/science.1213274 [PubMed: 22282804]
6. Dong YY, et al. K2P channel gating mechanisms revealed by structures of TREK-2 and a complex with Prozac. Science. 2015; 347:1256–1259. DOI: 10.1126/science.1261512 [PubMed: 25766236]
7. Bagriantsev SN, Clark KA, Minor DL Jr. Metabolic and thermal stimuli control K(2P)2.1 (TREK-1) through modular sensory and gating domains. EMBO J. 2012; 31:3297–3308. DOI: 10.1038/emboj.2012.171 [PubMed: 22728824]
8. Bagriantsev SN, Peyronnet R, Clark KA, Honore E, Minor DL Jr. Multiple modalities converge on a common gate to control K2P channel function. EMBO J. 2011; 30:3594–3606. emboj2011230 [pii]. DOI: 10.1038/emboj.2011.230 [PubMed: 21765396]
9. Schewe M, et al. A Non-canonical Voltage-Sensing Mechanism Controls Gating in K2P K(+) Channels. Cell. 2016; 164:937–949. DOI: 10.1016/j.cell.2016.02.002 [PubMed: 26919430]
10. Piechotta PL, et al. The pore structure and gating mechanism of K2P channels. EMBO J. 2011; 30:3607–3619. emboj2011268 [pii]. DOI: 10.1038/emboj.2011.268 [PubMed: 21822218]
11. Bagriantsev SN, et al. A high-throughput functional screen identifies small molecule regulators of temperature- and mechano-sensitive K2P channels. ACS chemical biology. 2013; 8:1841–1851. DOI: 10.1021/cb400289x [PubMed: 23738709]
12. Su ZW, Brown EC, Wang WW, MacKinnon R. Novel cell-free high-throughput screening method for pharmacological tools targeting K+ channels. P Natl Acad Sci USA. 2016; 113:5748–5753. DOI: 10.1073/pnas.1602815113
13. Brohawn SG, Campbell EB, MacKinnon R. Domain-swapped chain connectivity and gated membrane access in a Fab-mediated crystal of the human TRAAK K+ channel. Proc Natl Acad Sci U S A. 2013; 110:2129–2134. DOI: 10.1073/pnas.1218950110 [PubMed: 23341632]

14. Brohawn SG, Campbell EB, MacKinnon R. Physical mechanism for gating and mechanosensitivity of the human TRAAK K+ channel. Nature. 2014; 516:126–130. DOI: 10.1038/nature14013 [PubMed: 25471887]
15. Lolicato M, Riegelhaupt PM, Arrigoni C, Clark KA, Minor DL Jr. Transmembrane helix straightening and buckling underlies activation of mechanosensitive and thermosensitive K(2P) channels. Neuron. 2014; 84:1198–1212. DOI: 10.1016/j.neuron.2014.11.017 [PubMed: 25500157]
16. Cohen A, Ben-Abu Y, Hen S, Zilberberg N. A novel mechanism for human K2P2.1 channel gating. Facilitation of C-type gating by protonation of extracellular histidine residues. J Biol Chem. 2008; 283:19448–19455. M801273200 [pii]. DOI: 10.1074/jbc.M801273200 [PubMed: 18474599]
17. Sandoz G, Douguet D, Chatelain F, Lazdunski M, Lesage F. Extracellular acidification exerts opposite actions on TREK1 and TREK2 potassium channels via a single conserved histidine residue. Proc Natl Acad Sci U S A. 2009; 106:14628–14633. 0906267106 [pii]. DOI: 10.1073/pnas.0906267106 [PubMed: 19667202]
18. Bagneris C, et al. Prokaryotic NavMs channel as a structural and functional model for eukaryotic sodium channel antagonism. Proc Natl Acad Sci U S A. 2014; 111:8428–8433. DOI: 10.1073/pnas.1406855111 [PubMed: 24850863]
19. Tang L, et al. Structural basis for inhibition of a voltage-gated Ca2+ channel by Ca2+ antagonist drugs. Nature. 2016; 537:117–121. DOI: 10.1038/nature19102 [PubMed: 27556947]
20. Kearney PC, et al. Molecular Recognition in Aqueous-Media - New Binding-Studies Provide Further Insights into the Cation-Pi Interaction and Related Phenomena. Journal of the American Chemical Society. 1993; 115:9907–9919. DOI: 10.1021/ja00075a006
21. Hibbs RE, Gouaux E. Principles of activation and permeation in an anion-selective Cys-loop receptor. Nature. 2011; 474:54–60. DOI: 10.1038/nature10139 [PubMed: 21572436]
22. Yelshanskaya MV, et al. Structural Bases of Noncompetitive Inhibition of AMPA-Subtype Ionotropic Glutamate Receptors by Antiepileptic Drugs. Neuron. 2016; 91:1305–1315. DOI: 10.1016/j.neuron.2016.08.012 [PubMed: 27618672]
23. McClenaghan C, et al. Polymodal activation of the TREK-2 K2P channel produces structurally distinct open states. J Gen Physiol. 2016; 147:497–505. DOI: 10.1085/jgp.201611601 [PubMed: 27241700]
24. Chemin J, et al. A phospholipid sensor controls mechanogating of the K+ channel TREK-1. EMBO J. 2005; 24:44–53. 7600494 [pii]. DOI: 10.1038/sj.emboj.7600494 [PubMed: 15577940]
25. Chemin J, et al. Up- and down-regulation of the mechano-gated K(2P) channel TREK-1 by PIP (2) and other membrane phospholipids. Pflugers Arch. 2007; 455:97–103. DOI: 10.1007/s00424-007-0250-2 [PubMed: 17384962]
26. Murbartian J, Lei Q, Sando JJ, Bayliss DA. Sequential phosphorylation mediates receptor- and kinase-induced inhibition of TREK-1 background potassium channels. J Biol Chem. 2005; 280:30175–30184. M503862200 [pii]. DOI: 10.1074/jbc.M503862200 [PubMed: 16006563]
27. Patel AJ, et al. A mammalian two pore domain mechano-gated S-like K+ channel. Embo J. 1998; 17:4283–4290. DOI: 10.1093/emboj/17.15.4283 [PubMed: 9687497]
28. Maingret F, et al. TREK-1 is a heat-activated background K(+) channel. Embo J. 2000; 19:2483–2491. DOI: 10.1093/emboj/19.11.2483 [PubMed: 10835347]
29. Honore E, Maingret F, Lazdunski M, Patel AJ. An intracellular proton sensor commands lipid- and mechano-gating of the K(+) channel TREK-1. EMBO J. 2002; 21:2968–2976. DOI: 10.1093/emboj/cdf288 [PubMed: 12065410]
30. Fink M, et al. Cloning, functional expression and brain localization of a novel unconventional outward rectifier K+ channel. Embo J. 1996; 15:6854–6862. [PubMed: 9003761]
31. Veale EL, et al. Influence of the N terminus on the biophysical properties and pharmacology of TREK1 potassium channels. Molecular pharmacology. 2014; 85:671–681. DOI: 10.1124/mol.113.091199 [PubMed: 24509840]
32. Tertyshnikova S, et al. BL-1249 [(5,6,7,8-tetrahydro-naphthalen-1-yl)-[2-(1H-tetrazol-5-yl)-phenyl]-amine]: a putative potassium channel opener with bladder-relaxant properties. The Journal of pharmacology and experimental therapeutics. 2005; 313:250–259. DOI: 10.1124/jpet.104.078592 [PubMed: 15608074]

33. Hardy JA, Wells JA. Searching for new allosteric sites in enzymes. Current opinion in structural biology. 2004; 14:706–715. DOI: 10.1016/j.sbi.2004.10.009 [PubMed: 15582395]
34. Guizouarn H, Gabillat N, Motais R, Borgese F. Multiple transport functions of a red blood cell anion exchanger, tAE1: its role in cell volume regulation. J Physiol. 2001; 535:497–506. PHY_12115 [pii]. [PubMed: 11533139]
35. Rapp C, Goldberger E, Tishbi N, Kirshenbaum R. Cation-pi interactions of methylated ammonium ions: A quantum mechanical study. Proteins-Structure Function and Bioinformatics. 2014; 82:1494–1502. DOI: 10.1002/prot.24519
36. Crowley PB, Golovin A. Cation-pi interactions in protein-protein interfaces. Proteins-Structure Function and Bioinformatics. 2005; 59:231–239. DOI: 10.1002/prot.20417
37. Payandeh J, Minor DL Jr. Bacterial Voltage-Gated Sodium Channels (BacNas) from the Soil, Sea, and Salt Lakes Enlighten Molecular Mechanisms of Electrical Signaling and Pharmacology in the Brain and Heart. Journal of molecular biology. 2014
38. Zhou Y, Morais-Cabral JH, Kaufman A, MacKinnon R. Chemistry of ion coordination and hydration revealed by a K+ channel-Fab complex at 2.0 A resolution. Nature. 2001; 414:43–48. [PubMed: 11689936]
39. Kawate T, Gouaux E. Fluorescence-detection size-exclusion chromatography for precrystallization screening of integral membrane proteins. Structure. 2006; 14:673–681. [PubMed: 16615909]
40. Drew D, et al. GFP-based optimization scheme for the overexpression and purification of eukaryotic membrane proteins in Saccharomyces cerevisiae. Nat Protoc. 2008; 3:784–798. nprot. 2008.44 [pii]. DOI: 10.1038/nprot.2008.44 [PubMed: 18451787]
41. Newstead S, Kim H, von Heijne G, Iwata S, Drew D. High-throughput fluorescent-based optimization of eukaryotic membrane protein overexpression and purification in Saccharomyces cerevisiae. Proc Natl Acad Sci U S A. 2007; 104:13936–13941. 0704546104 [pii]. DOI: 10.1073/pnas.0704546104 [PubMed: 17709746]
42. Kirchhofer A, et al. Modulation of protein properties in living cells using nanobodies. Nature Structural & Molecular Biology. 2010; 17:133-U162.
43. Shaya D, et al. Voltage-gated sodium channel (NaV) protein dissection creates a set of functional pore-only proteins. Proc Natl Acad Sci U S A. 2011; 108:12313–12318. 1106811108 [pii]. DOI: 10.1073/pnas.1106811108 [PubMed: 21746903]
44. Kabsch W, Xds. Acta crystallographica. Section D, Biological crystallography. 2010; 66:125–132. DOI: 10.1107/S0907444909047337 [PubMed: 20124692]
45. Evans PR, Murshudov GN. How good are my data and what is the resolution? Acta crystallographica. Section D, Biological crystallography. 2013; 69:1204–1214. DOI: 10.1107/S0907444913000061 [PubMed: 23793146]
46. Diederichs K, Karplus PA. Better models by discarding data? Acta crystallographica. Section D, Biological crystallography. 2013; 69:1215–1222. DOI: 10.1107/S0907444913001121 [PubMed: 23793147]
47. Karplus PA, Diederichs K. Linking crystallographic model and data quality. Science. 2012; 336:1030–1033. DOI: 10.1126/science.1218231 [PubMed: 22628654]
48. Emsley P, Cowtan K. Coot: model-building tools for molecular graphics. Acta crystallographica Section D, Biological crystallography. 2004; 60:2126–2132. [PubMed: 15572765]
49. Collaborative Computational Project N. The CCP4 suite: Programs for protein crystallography. Acta crystallographica. Section D, Biological crystallography. 1994; 50:760–763. [PubMed: 15299374]
50. Adams PD, et al. PHENIX: a comprehensive Python-based system for macromolecular structure solution. Acta crystallographica. Section D, Biological crystallography. 2010; 66:213–221. DOI: 10.1107/S0907444909052925 [PubMed: 20124702]
51. Chen VB, et al. MolProbity: all-atom structure validation for macromolecular crystallography. Acta crystallographica. Section D, Biological crystallography. 2010; 66:12–21. DOI: 10.1107/S0907444909042073 [PubMed: 20057044]
52. Pascale R, et al. New N-(phenoxydecyl)phthalimide derivatives displaying potent inhibition activity towards alpha-glucosidase. Bioorg Med Chem. 2010; 18:5903–5914. DOI: 10.1016/j.bmc.2010.06.088 [PubMed: 20667739]

53. Eguchi Y, Sasaki F, Sugimoto A, Ebisawa H, Ishikawa M. Studies on Hypotensive Agents - Synthesis of 1-Substituted 3-(2-Chlorophenyl)-6-Ethoxycarbonyl-5,7-Dimethyl-2,4(1h,3h)-Quinazolinediones. Chem Pharm Bull. 1991; 39:1753–1759. [PubMed: 1777928]

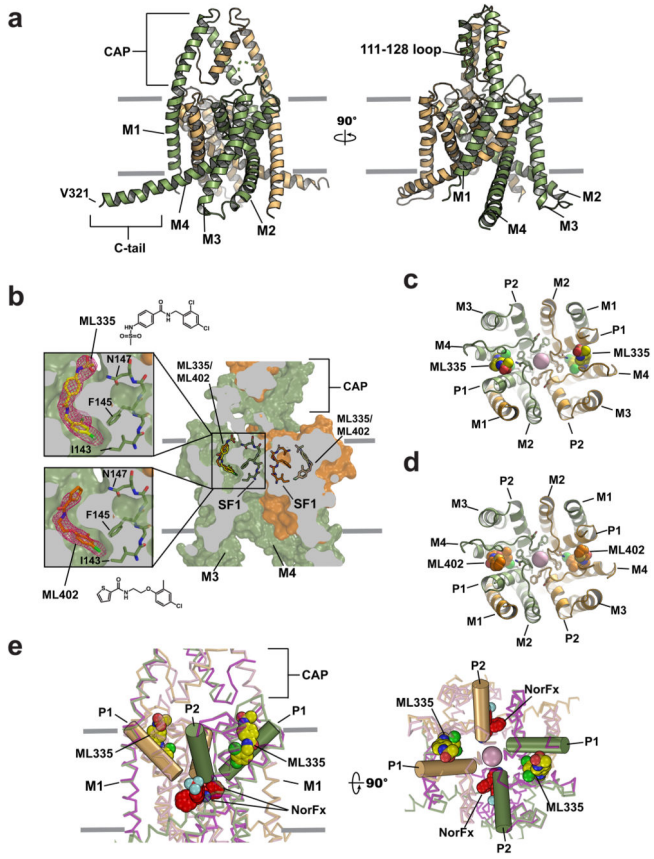

Figure 1. K_{2P}2.1(TREK-1) structures

a, $K_{2P}2.1(TREK\text{-}1)_{cryst}$ cartoon (smudge and light orange) smudge subunit extracellular cap domain (CAP), M1–M4 transmembrane helices, C-tail, and V321 are labeled. **b,** K_{2P} modulator pocket cutaway. Cutouts display ML335 and ML402 F_o-F_c densities (3.0σ). ML335, ML402, and Selectivity Filter 1 (SF1) are sticks. **c,** and **d**, Extracellular views excluding the CAP domain of **c,** ML335 and **d,** ML402 binding sites. ML335 and ML402 are space filling. Selectivity filter sidechains are sticks. **e,** Wire representation comparing K_{2P}2.1(TREK-1):ML335 (smudge and light orange) and K_{2P}10.1(TREK-2):norfluoxetine[6] (light pink and magenta) binding sites. K_{2P}2.1(TREK-1) P1 and P2 are cylinders. ML335 (yellow) and norfluoxetine (NorFx) (red) are space filling. In all panels select residues and channel elements are indicated, and where present, grey lines indicate the membrane.

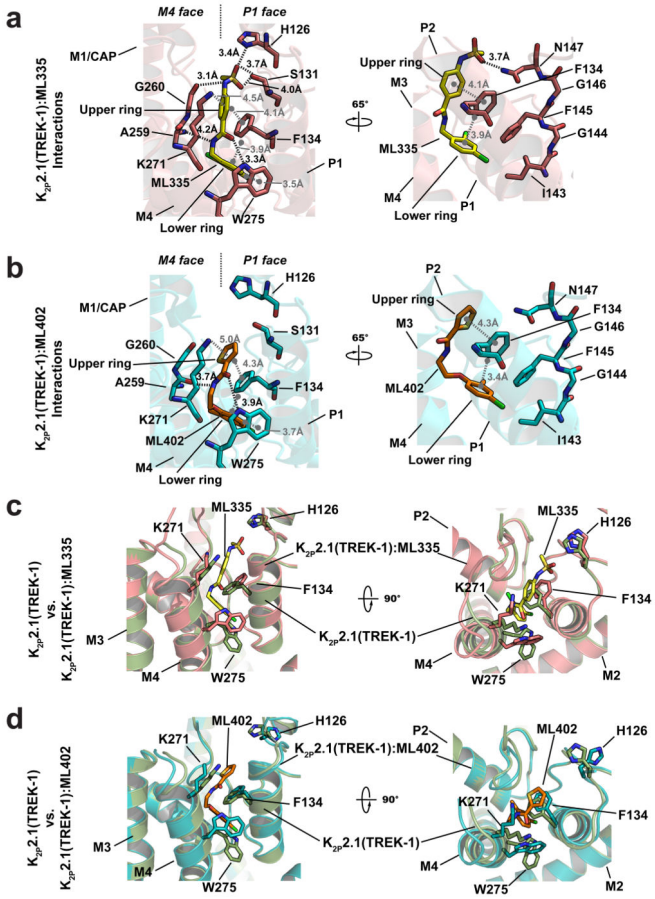

Figure 2. K_{2P}2.1(TREK-1) activator interactions

Cartoon diagram of **a,** K_{2P}2.1(TREK-1):ML335 and **b,** K_{2P}2.1(TREK-1):ML402 interactions. Electrostatic and hydrogen bond interactions are black. Cation-π and π-π interactions are grey. **c,** and **d**, comparison of K_{2P}2.1(TREK-1) (smudge) with **c,** K_{2P}2.1(TREK-1):ML335 (deep salmon) and **d**, K_{2P}2.1(TREK-1):ML402 (cyan).

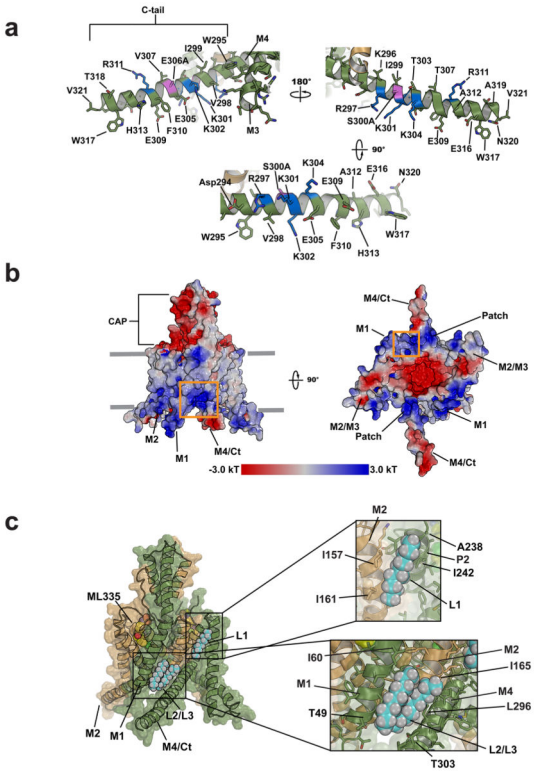

Figure 3. $K_{2P}2.1$(TREK-1) C-tail and lipid binding sites

a, $K_{2P}2.1$(TREK-1) C-tail. Positively charged residues are blue. S300A and E306A, a site having slight distortion from helical geometry, are magenta. **b,** $K_{2P}2.1$(TREK-1) Electrostatic surface potential. Orange box highlights M1/M2/M4 junction. Cytoplasmic view (left) indicates C-tail positively charged patch. **c,** Lipids L1, L2, and L3 (cyan and white) shown as space filling. ML335 (yellow) is indicated. Insets show lipid binding pocket details.

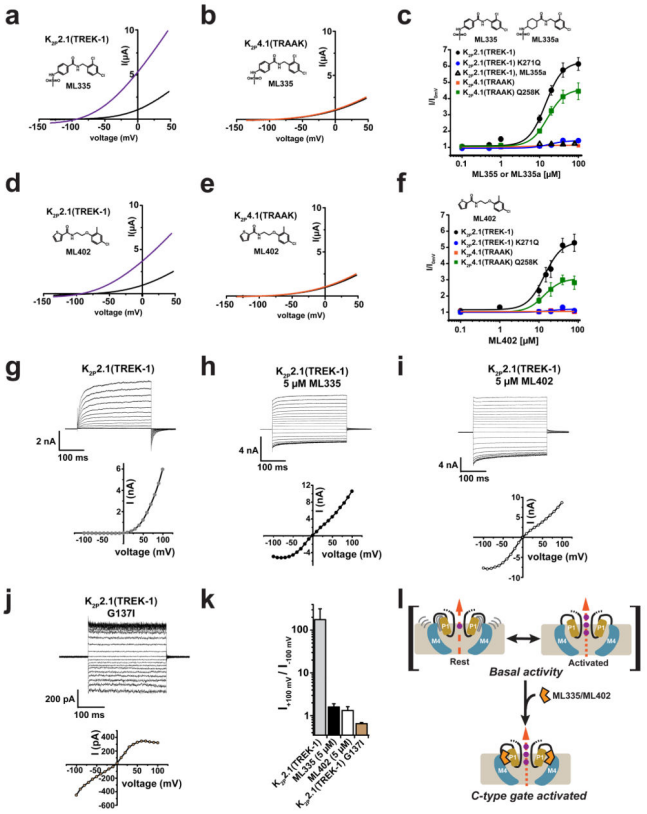

Figure 4. K_{2P}2.1(TREK-1) activator function

Exemplar current traces for **a,** K_{2P}2.1(TREK-1) (black) with 20 μM ML335 (purple). **b,** K_{2P}4.1(TRAAK) (black) with 50 μM ML335 (orange). **c,** ML335 dose response curves for K_{2P}2.1(TREK-1) (black), EC_{50}=14.3 ± 2.7 μM (n≥5); K_{2P}2.1(TREK-1) K271Q (blue filled circles); K_{2P}4.1(TRAAK) (orange); K_{2P}4.1(TRAAK) Q258K (green) EC_{50}=16.2 ± 3.0 μM (n≥4); and ML335a: K_{2P}2.1(TREK-1) (black open triangles). Exemplar current traces for **d,** K_{2P}2.1(TREK-1) (black) with 20 μM ML402 (purple). **e,** K_{2P}4.1(TRAAK) (black) with 50 μM ML335 (orange). **f,** ML402 dose response curves for K_{2P}2.1(TREK-1) (black), EC_{50}=13.7 ± 7.0 μM (n≥3); K_{2P}2.1(TREK-1) K271Q (blue); K_{2P}2.1(TREK-1) (blue); K_{2P}4.1(TRAAK) (orange); K_{2P}4.1(TRAAK) Q258K (green) EC_{50}=13.6 ± 1.5 μM (n≥3). **g–j,** Exemplar current traces and voltage-current relationships for indicated K_{2P}s in HEK293 inside-out patches in 150 mM $K^+_{[out]}$/150 mM $Rb^+_{[in]}$ for **g**, K_{2P}2.1(TREK-1), **h**, K_{2P}2.1(TREK-1) with 5 μM ML335, **I,** K_{2P}2.1(TREK-1) with 5 μM ML402, and **j**, K_{2P}2.1(TREK-1) G137I. **k,** Rectification coefficients (I_{+100mV}/I_{-100mV}) from recordings (n≥3) made in '**g–j'. l,** TREK activation model. Grey lines indicate mobile P1 (tan) and M4 (blue). C-type activators (orange), stabilize the selectivity filter and channel 'leak mode'. Potassium ions are purple. Gap in arrows indicates current flow intensity. Membrane is grey.